

Chaotic and Arnold stripes in weakly chaotic Hamiltonian systems

M. S. Custódio¹, C. Manchein² and M. W. Beims¹

¹*Departamento de Física, Universidade Federal do Paraná, 81531-990 Curitiba, Brazil and*

²*Departamento de Física, Universidade do Estado de Santa Catarina, 89219-710 Joinville, Brazil*

(Dated: May 3, 2019)

The dynamics in weakly Hamiltonian chaotic systems strongly depends on initial conditions and little can be affirmed about generic behaviors. Using two distinct Hamiltonian systems, namely one particle in an open rectangular billiard and four particles globally coupled on a discrete lattice, we show that in these models weak chaos emerges inside chaotic stripes. The stripes represent intervals of initial conditions which generate chaotic motion and increase with the nonlinear parameter of the system. In the billiard case the initial conditions are the injection angles. For higher-dimensional systems and small nonlinearities the stripes are the initial condition inside which Arnold diffusion occurs.

PACS numbers: 05.45.-a, 05.45.Ac

Keywords: Open billiards, self-similarity, chaos, stickiness, Arnold diffusion.

Starting from integrable Hamiltonian systems, we show that weakly nonintegrable perturbations solely generate chaotic motion inside specific intervals of initial conditions. These intervals increase with the magnitude of the perturbation creating stripes of chaotic motion. Totally chaotic motion is obtained for larger perturbations *via* the overlap of stripes. Results are shown for one particle inside an open rectangular billiard with rounded corner and four particles coupled globally on a discrete lattice. For higher-dimensional systems the stripes are the chaotic channels where Arnold diffusion occurs and are designed as Arnold stripes.

I. INTRODUCTION

The precise description of weak chaos in nonintegrable high-dimensional Hamiltonian system is not trivial. When starting from an integrable system, the large amount of regular structures (invariant tori in two dimensions) which remain for small nonlinear perturbations strongly influences the dynamics [1]. The present contribution shows a simple and clarifying way to analyze the dynamics for small perturbations where weak chaos is dominant. The dynamics dependence on initial conditions (ICs) is shown in the plot: ICs *versus* the nonlinear parameter. The chaotic motion is generated inside stripes of ICs which get larger as the nonlinear parameter increases. Results are shown for two different Hamiltonian systems. The first one is the two dimensional open rectangular billiard with rounded corners. Such open billiard, but with straight corners and a rounded open channel, was studied recently [2]. It was shown that the rounded open channel generates a chaotic dynamics inside the stripes and thus inside the billiard. The chaotic motion was characterized based on exponential decays of escape times (ETs) statistics [3] inside the stripes. Unusual boundary conditions in two-dimensional billiards

have been studied in recent years, as for example, edge roughness in quantum dots [4], unusual boundary conditions in two-dimensional billiards [5, 6], soft billiards [7–10], edge corrections [11] in a resonator, effects of soft walls [12], rounded edges [13, 14], deformation of dielectric cavities [15], location of the hole [16], among others.

The second example considered here comes from the nonlinear dynamics, namely 4 particles which are globally coupled on a discrete lattice. This system was extensively studied in [17–19], and the dynamics characterized by the existence of an ordering process called clustering. In the context of the present work, this model serves to show that chaotic stripes exist in a higher-dimensional and are related to the Arnold web, or stochastic web [20]. Different from the billiard case, the chaotic motion will be characterized by the Finite Time Lyapunov Exponent (FTLE). Starting from a chaotic trajectory, regular structures induce sticky motion [21, 22], the convergence of the FTLEs is affected and the dynamics becomes dependent on ICs. Recent methods [12, 23–27], which use higher-order cumulants of Gaussian-like distributions of the FTLEs to characterize the whole dynamics via sticky motion, do not work quite well for very small nonlinear perturbations since the distributions may be multimodal [28].

The paper is organized as follows. Section II presents the model of the open billiard system and shows numerical results for the ETs decays and the existence of stripes in emission angles. Section III presents the coupled map lattice model, shows the existence of the stripes and their relation to the Arnold web. In Section IV we present our final remarks.

II. STRIPES IN OPEN BILLIARDS

The model used is shown in Fig. 1, which is a rectangular billiard with dimension $L \times D$. The four corners are assumed to be rounded with radius R . For $R/L = 0$ the initial angles and exit time of the short-

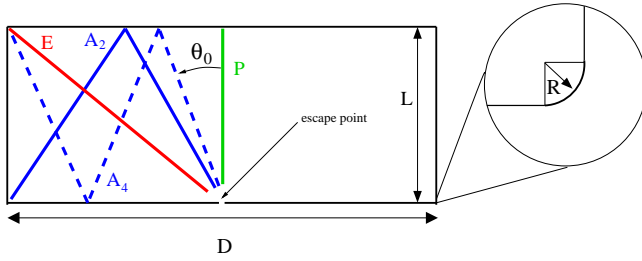


FIG. 1. (Color online) The rectangular billiard, with dimension $L \times D$, has four rounded corners (with radius R , see magnification of just one border). The escape point with aperture a lies exactly in the middle of the billiard. Initial angle θ_0 and, schematically, the shortest escape trajectories (P, E, A_2, A_4 and A_6) are shown. In all simulations we use $L = 4$ and $D = 10$.

est orbits P, E, A_2, A_4 and A_6 , shown schematically in Fig. 1, can be obtained analytically. The initial angles are $\theta_0^{(n)} = \arctan[\frac{D}{2nL}]$ and for the close billiard they have period $q = 2^n$ ($n = 1, 2, 3, \dots$). The corresponding ETs are $t_n = nt$, where t is the ET from the case $n = 1$, explained below. The particle which collides perpendicularly against the wall in front of the escape hole and then leaves the billiard [see trajectory P in Fig. 1 has the shortest ET $t_0 \sim 8.0$ and initial angle $\theta_0 \sim 0.0$]. The next shortest ETs ($t_1 = t \sim 12.8$) occurs for $n = 1$ at $\theta^{(1)} = \arctan 5.0/4.0 \sim 0.89$, where the particle collides directly with the corner of the billiard. See trajectory E in Fig. 1. Trajectory A_2 in Fig. 1 has an ETs $\sim 2t$ and initial angle $\theta^{(2)} = \arctan 5.0/8.0 \sim 0.56$. In the limit $\theta_0 \rightarrow \pi/2$ the ETs tend to increase since the trajectories are parallel to the escape point.

The closed rectangular billiard is integrable in the absence of corner effects ($R = 0$). All Lyapunov exponents are zero and the dynamics can be described in terms of invariant tori. Such regular dynamics is shown in the phase-space of Fig. 2(a), where the collision angle θ is plotted as a function of horizontal coordinate x . Tori with irrational winding numbers are the straight lines parallel to the x -axis. Tori with rational winding numbers are periodic orbits and are the marginally unstable periodic orbits (MUPOs) from this problem. When opening up the billiard, ICs which start on an irrational torus will certainly escape the billiard after some time, but trajectories which start exactly on a rational tori will never leave the billiard, except for those ICs which match the opening channel. Figure 2(b) shows the phase-space dynamics when $R/L = 0.1$ starting from one IC $\theta_0 = 0.86$. Blue points are related to points along the trajectory which collide with vertical and horizontal parallel straight walls, while green points are those which collide with the rounded corner. What happens is that the trajectory starts on an irrational torus, travels along this torus (blue horizontal lines) until it collides with one of the rounded corners (green points) and is scattered there to a new tori. It travels on this new tori until

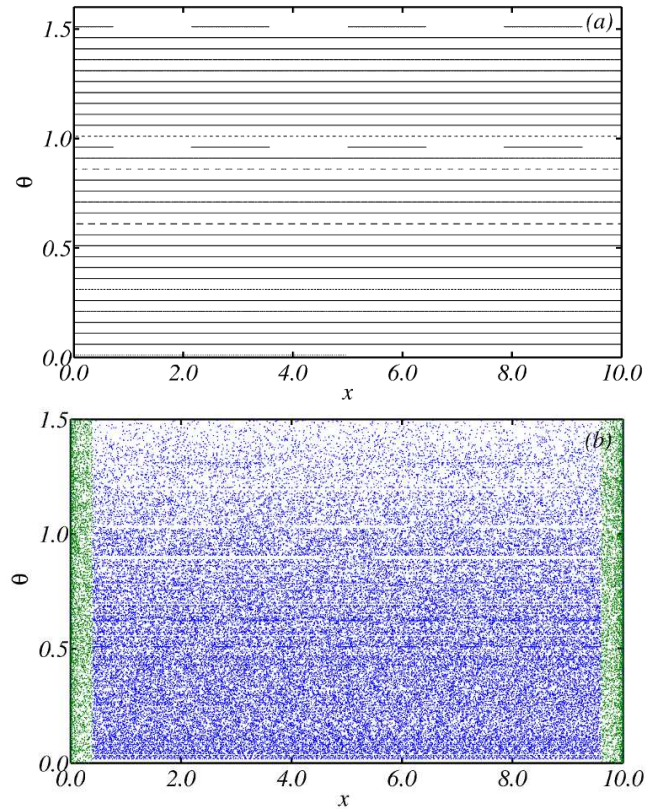


FIG. 2. (Color online) Phase-space dynamics for (a) $R = 0$ and (b) $R/L = 0.1$ (one IC): Green (light gray) points occur when the trajectory collides with the rounded corner and defines the scattering region (SR) or chaotic region. Blue (dark gray) points occur when the trajectory collides with the vertical and horizontal parallel walls.

it is scattered again to another tori. This procedure repeats itself until the whole phase space is filled. This is exactly what happens in Fig. 2(b), obtained using just one initial condition. The rounded corner is called scattering region (SR) and generates the chaotic dynamics. Although there are no regular islands in phase space, sticky motion occurs due to the existence of MUPOs, as explained in details in [2].

In order to analyze the effect of rounded corners on the emission angles dynamics we start simulations at times $t = 0$ from the open channel, uniformly distributed from $x_0 = D/2$, with an initial angle θ_0 towards the inner part of the billiard with velocity $|\vec{v}| = 1$. Elastic collisions are assumed at the billiard boundaries and at the rounded corners of the open channel. For each of the 10^5 IC distributed uniformly in the interval $0.01 \lesssim \theta_0 \lesssim 1.57$ we wait until the particle leaves the billiard and record θ_f . In all cases $a = 0.4$.

The complex dynamics generated by the rounded corners becomes apparent when the escape angles θ_f are plotted as function of the initial incoming angle θ_0 and for different ratios R/L . This is shown in Fig. 3 which

was obtained by using 1000×1000 points in the interval $0.002 \leq R/L \leq 0.35$ [$-6.0 \leq \log(R/L) \leq -1.0$]. Figure

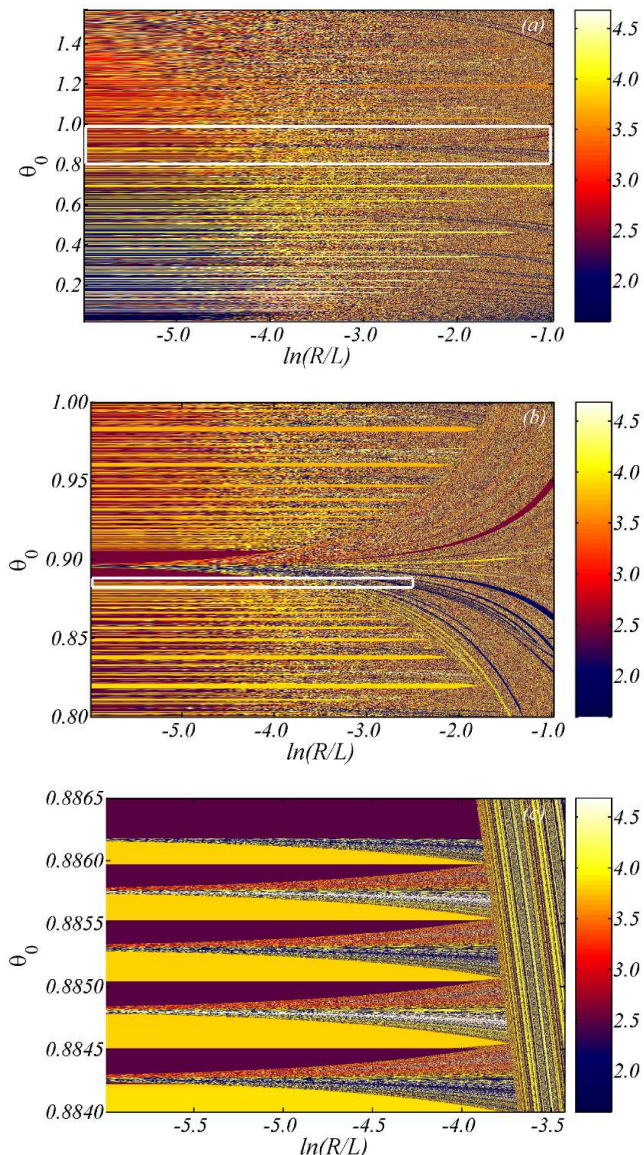


FIG. 3. (Color online) (a) Escape angle as a function of $\log(R/L)$ and θ_0 , (b) and (c) are magnifications.

3(a) shows θ_f as a function of $\log(R/L)$ and θ_0 . Each color is related to one emission angle θ_f (see the colorbar on the right: dark blue \rightarrow red \rightarrow yellow \rightarrow white in the colorscale and dark gray to white in the grayscale). These emission angles vary between $\theta_f \sim 1.4$ (almost horizontally to the left) and $\theta_f \sim 4.5$ (almost horizontally to the right). Stripes with different colors are evident for a significant range of R/L values. Each stripe is defined by a bunch of ICs which leave to the same θ_f . As R/L increases more and more, some stripes survive while others are destroyed or mixed. The emission angles show a very rich dynamics due to the increasing rounded corners,

alternating between all possible colors.

Figure 3(b) shows a magnification from Fig. 3(a). The magnification is taken around a main stripe related to the trajectory E ($\theta_0 \sim 0.89$) shown in Fig. 1. We observe that a large stripe (secondary) emerges symmetrically from the middle of this main stripe. Inside this secondary stripe, numerous distinct escape angles are observed. The width of this secondary stripe increases linearly with R/L . Outside the main stripe a large amount of smaller structures with distinct angles can be observed. In order to show this in more details and to explain the physics involved in the emission angles, we discuss next a magnification of Fig. 3(b) (see black box). This is shown in Fig. 3(c), where a sequence of secondary stripes appear on the light blue (gray) background. The width of each stripe in this sequence increases with R/L , remembering stripes from a backgammon board [2]. ICs which start inside the backgammon stripe collide, at least once, with the rounded corner so that distinct emission angles can be observed. Different from what is observed from border effects [2], here the sequence of backgammon stripes in Fig. 3(b), and the corresponding multicolor backgammon stripes from Fig. 3(c), are *not* born at the boundary between the purple (black) and orange (white) escape angles at $R/L \sim 0$. The rich and complex dynamics is always generated from ICs starting inside the backgammon stripes, so that a large amount of different colors in the emission angles appears, showing that tiny changes or errors in the initial angle may drastically change the emission angle. The location of the backgammon stripes itself is not self-similar, but *inside* the backgammon stripes the self-similar structure is evident. Backgammon stripes which emerge at different initial angles at $R/L \sim 0.0$ increase their width with R/L and start to overlap for $R/L \sim 0.05$, where the dynamics of strongly sensitive to initial angles θ_0 . The width of the stripes increase with R/L and allows us to characterize the different domains of the dynamics.

The dynamics generated by starting with IC *inside* the backgammon stripes is the consequence of trajectories which collide with the rounded corner and the chaotic motion appears. This can be demonstrated via the ETs statistic defined [29] by $Q(\tau) = \lim_{N \rightarrow \infty} \frac{N_\tau}{N}$, where N is the total number of recurrences and N_τ is the number of recurrences with time $T \geq \tau$. The time T is recorded when the trajectory returns to the recurrence region, which is the open channel. In chaotic hyperbolic systems the ETs statistic decays exponentially while systems with stickiness it decays as a power law $Q(\tau) \propto \tau^{-\gamma_{esc}}$ with $\gamma_{esc} > 1$ being the scaling exponent. Usually it is assumed to have stickiness when a power-law decay with $\gamma_{esc} > 1$ is observed for two decades in time. Power-law decays with $\gamma_{esc} = 1$ [2, 30] appear in integrable systems, which is the case of our model when $R/L = 0$. Figure 4 displays in a semi-log plot the quantity $Q(\tau)$ obtained using different values of the ratio $R/L = 0.0, 1.0 \times 10^{-4}, 1.0 \times 10^{-3}, 1.0 \times 10^{-2}, 5.0 \times 10^{-2}$, where L is kept fixed. ICs are $0.00001 \leq \theta_0 \leq 1.5700$ and

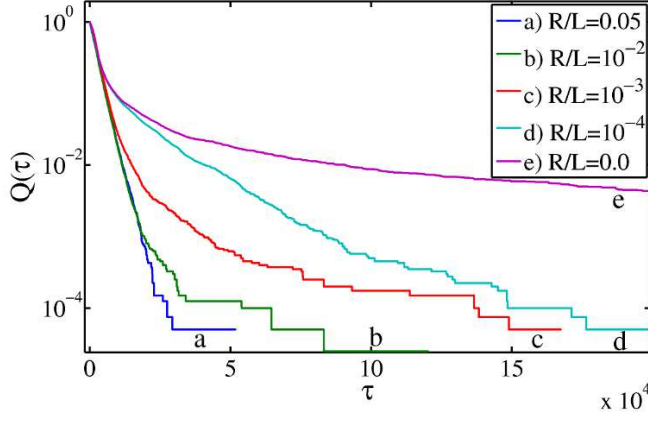


FIG. 4. (Color online) Semi-log plot of $Q(\tau)$ for distinct values of R/L .

$-0.00001 \leq \theta_0 \leq -1.5700$. Straight lines in this plot are exponential decays. For the integrable case $R/L = 0.0$ (curve e) a power law decays occurs with $\gamma_{esc} \sim 1$. Trajectories close to the periodic orbits inside the rectangle generate the power-law decay with $\gamma_{esc} = 1$. Small corner effects, $R/L = 10^{-4} \rightarrow 10^{-3}$ (see curves $d \rightarrow c$), change the qualitative behavior of $Q(\tau)$ so that regular trajectories close to MUPOs generate, for small period of times, a power-law decay with $1 < \gamma_{esc} < 2$. For a detailed discussion of a similar behavior we refer the reader to [2]. However, for $R/L = 1.0 \times 10^{-2}$ [$\log(R/L) = -4.6$], 0.05 [$\log(R/L) = -3.0$] (curves b, a), which correspond to values from Fig. 3(c), a straight line decay is observed, characterizing the transition to chaotic motion when stripes become larger and larger.

III. STRIPES IN COUPLED MAPS

At next we analyze the IC dependence of the dynamics of 4 particles globally coupled on a discrete lattice. It has a 8-dimensional phase space and particles are coupled on a unit circle, where the state of each particle is defined by its position $2\pi x^{(i)}$ and its conjugate momentum $p^{(i)}$. The dynamics on the lattice obeys [17]

$$\begin{cases} p_{t+1}^{(i)} = p_t^{(i)} + \frac{K}{2\pi\sqrt{3}} \sum_{j=1, j \neq i}^{N=4} \sin[2\pi(x_t^{(j)} - x_t^{(i)})], \\ x_{t+1}^{(i)} = x_t^{(i)} + p_{t+1}^{(i)}, \end{cases} \quad (1)$$

where mod 1 must be taken in the variables $p^{(i)}, x^{(i)}$, and $i = 1, \dots, N = 4$. For $K > 0$ the interaction between two particles i and j is attractive [18]. For this coupling the total momentum $P_T = \sum_{j=1}^{N=4} p_t^j$ is preserved.

An interesting way to describe the complicated dynamics dependence on ICs is shown in the plot ($K \times p_0^{(2)}$) from Fig. 5. In colors are the largest FTLEs after 10^4 iterations. Initial conditions are chosen on the invariant

structure $P_T = 0.0$ and $X_{CM} = 0.0$. This plot shows, as a function of K , those ICs $p_0^{(2)}$ which generate the regular, mixed or chaotic motion. While black colors describe initial conditions with generate a regular motion, with zero FTLEs, cyan, red to yellow colors are obtained from ICs which generate increasing positive FTLEs. A rich

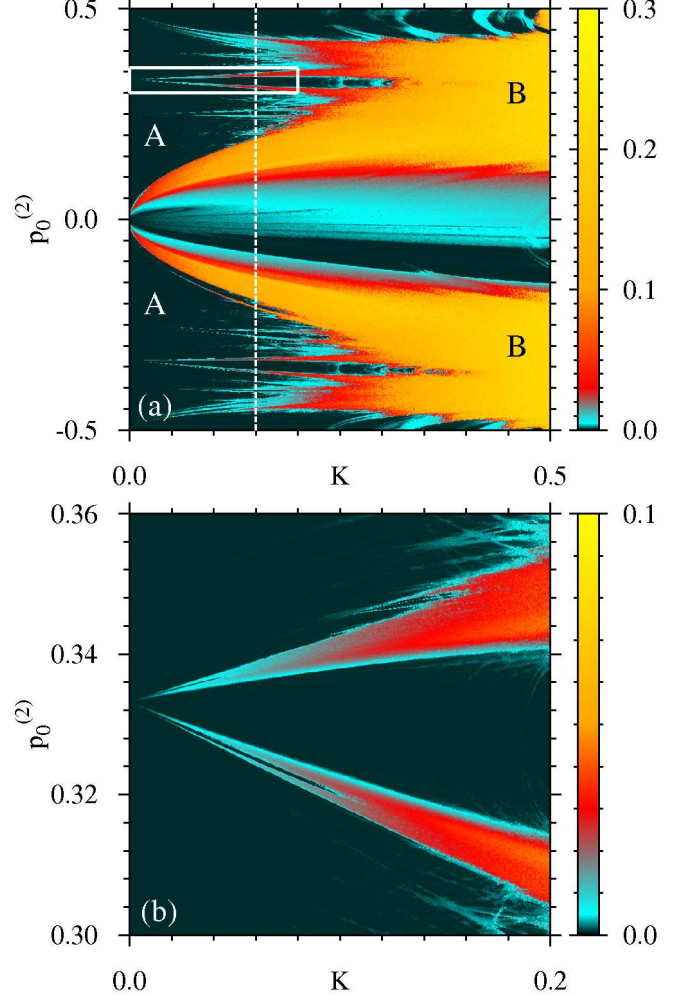


FIG. 5. (Color online) Grid of 1000×1000 points with the FTLEs as a function of $K \times p_0^{(2)}$.

variety of structures is observed. Essentially two distinct larger regions of motions are observed and demarked in the plot as: (A) where FTLEs are smaller and (B) where FTLEs are larger. In between the FTLEs mix themselves along complicated and apparently fractal structures. For $K \rightarrow 0$ FTLEs also go to zero inside region (A). However there are some stripes, which emanate from $K \sim 0$ for which FTLEs are larger. Two larger stripes are born close to $p_0^{(2)} \sim 0.0$ and growth symmetrically around this point as K increases. Along the line $p_0^{(2)} \sim 0.0$ the dynamics is almost regular for $K < 1$, becoming chaotic for larger values of K . This picture shows us clearly that

for the same K value, different ICs (in this case $p_0^{(2)}$) have distinct FTLEs. Zero FTLEs are related to regular trajectories, larger FTLEs are related to chaotic trajectories and intermediate FTLEs are related to chaotic trajectories which touched, for a finite time, the regular structures from the high-dimensional phase space. Such regular structures can be global invariants (as P_T) or local, or collective ordered states which live in the high-dimensional phase space. As trajectories itinerate between ordered and random states, the regular structures affect locally the FTLEs inducing sticky motion, so that the corresponding FTLEs decrease. Thus each point in the mixed plot from Fig. 5(a) with and intermediate FTLE for a fixed K value, is necessarily related to a trajectory which suffers sticky motion. Figure 5(b) is a magnification of Fig. 5(a) and shows similar stripes structures observed in the billiard case. As the nonlinear parameter K increases, the width of the stripes increase and they start to overlap, generating the totally chaotic motion for higher K values (not shown).

It is very interesting to observed that the stripes define the channels of chaotic motion which form the Arnold web [20] which allows the Arnold diffusion to occur in higher-dimensional systems. This can be better understood when the FTLEs are plotted in the phase space projection $p_0^{(1)} \times p_0^{(2)}$, shown in Fig. 6 for $K = 0.15$ [see dashed line in Fig.5(a)]. Black points are related

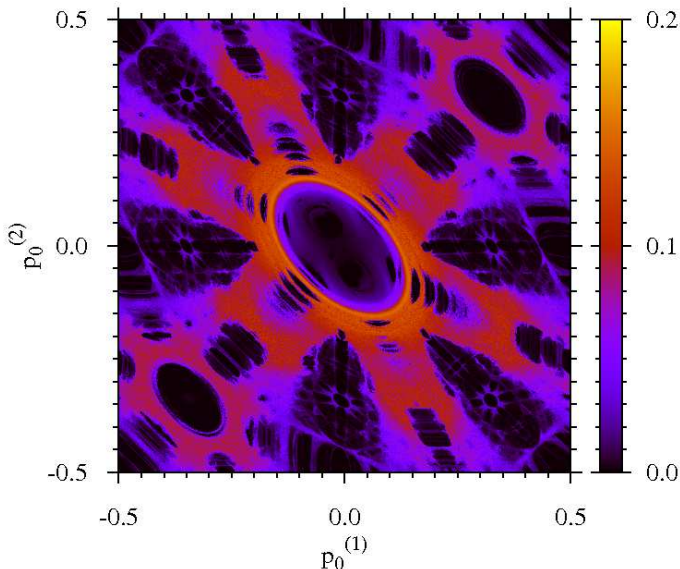


FIG. 6. (Color online) FTLEs in the phase space projection $p_0^{(1)} \times p_0^{(2)}$ for $K = 0.15$.

to close to zero FTLEs while purple to red points are related to increasing FTLEs. This picture is similar to the one shown in [19] (but in black and white), and presents a form called as “onion”. In fact, this plot shows an Arnold web, or stochastic web, where points with larger FTLEs are the chaotic channels inside which the Arnold diffusion occurs. The projection of points from the line $p_0^{(1)} = 0.0$ in Fig. 6 along the axis $p_0^{(2)}$, gives exactly the points from the white dashed line in Fig. 5(a). Thus the stripes in Fig. 5 show directly how the Arnold web changes with K and where the chaotic channels are born.

IV. CONCLUSIONS

Chaotic stripes are shown to exist in two distinct weak chaotic Hamiltonians systems, namely an open rectangular billiard with rounded corners and 4 globally coupled particles on a discrete lattice. The width of the stripes increase with the nonlinear parameter and allow us to characterize the different domains of the dynamics. For the billiard case the stripes define injection angles which generate an chaotic dynamics inside the billiard and an uncertainty about ejection angles. For small values of the nonlinear parameter but higher-dimensional systems, the stripes are the chaotic channels in the Arnold web inside which the Arnold diffusion occurs [20]. From this perspective we can define the chaotic stripes as *Arnold stripes*. We also observed such stripes for Hamiltonian systems with higher values of $N > 4$ and other couplings (not shown here). This suggests that weak chaos in Hamiltonian systems always emerges inside stripes of particular ICs. This is of relevance since in such systems finite time distributions, independently of the considered physical quantity, are not Gaussians anymore and decay rates of recurrences and time correlations are difficult to obtain [25, 26]. For higher values of the nonlinear parameters a totally chaotic motion is observed due to the overlap of Arnold stripes.

ACKNOWLEDGMENTS

The authors thank CNPq, CAPES and FINEP (under project CT-INFRA/UFPR) for partial financial support.

[1] A. J. Lichtenberg and M. A. Lieberman, *Regular and Chaotic Dynamics* (Springer-Verlag, 1992).

[2] M. S. Custodio and M. W. Beims, Phys. Rev. E **83**, 056201 (2011).

- [3] E. G. Altmann, A. E. Motter, and H. Kantz, Phys. Rev. E **73**, 026207 (2006).
- [4] F. Libisch, C. Stampfer, and J. Burgdörfer, Phys. Rev. B **79**, 115423 (2009).
- [5] E. Bogomolny, M. R. Dennis, and D. Dubertrand, J. Phys. A **41**, 335102 (2009).
- [6] M. V. Berry and M. R. Dennis, J. Phys. A **41**, 135203 (2008).
- [7] H.A.Oliveira, G.A.Emidio, and M.W.Beims (arXiv:1111.1966).
- [8] P. Baldwin, Physica D **29**, 321 (1988).
- [9] A. Knauf, Physica D **36**, 259 (1989).
- [10] D. Turaev and V. Rom-Kedar, J. Stat. Phys. **112**, 765 (2003).
- [11] C. Vaa, P. M. Koch, and R. Blümel, Phys. Rev. E **72**, 056211 (2005).
- [12] H. A. Oliveira, C. Manchein, and M. W. Beims, Phys. Rev. E **78**, 046208 (2008).
- [13] M. S. Custodio and M. W. Beims, Journal of Physics: Conference Series **246**, 012004 (2010).
- [14] J. Wiersig, Phys. Rev. A **67**, 023807 (2003).
- [15] R. Dubertrand, E. Bogomolny, N. Djellali, M. Lebental, and C. Schmit, Phys. Rev. A **77**, 013804 (2008).
- [16] L. Bunimovich and A. Yutchenko, Israel J. of Math. at press, arXiv:0811.4438v1 (2010).
- [17] T.Konishi and K.Kaneko, J.Phys.A **23**, 715 (1990).
- [18] T.Konishi and K.Kaneko, J.Phys.A **1992**, 6283 (1992).
- [19] K.Kaneko and T.Konishi, Physica D **71**, 146 (1994).
- [20] G. M. Zaslavsky, *Hamiltonian chaos and fractional dynamics* (Oxford, University Press, 2008).
- [21] G.Contopoulos and M.Harsoula, Int.J.Bif.Chaos **20**, 2005 (2010).
- [22] G. M. Zaslavski, Phys. Rep. **371**, 461 (2002).
- [23] S. Tomsovic and A. Lakshminarayan, Phys. Rev. E **76**, 036207 (2007).
- [24] M. W. Beims, C. Manchein, and J. M. Rost, Phys. Rev. E **76**, 056203 (2007).
- [25] C. Manchein, M. W. Beims, and J. M. Rost, arXiv:0907.4181 (2011).
- [26] R. Artuso and C. Manchein, Phys. Rev. E **80**, 036210 (2009).
- [27] C. Manchein and M. W. Beims, Chaos Solitons & Fractals **39**, 2041 (2009).
- [28] J. D. Szezech, S. R. Lopes, and R. L. Viana, Phys. Lett. A **335**, 394 (2005).
- [29] E. G. Altmann, A. Motter, and H. Kantz, CHAOS **15**, 033105 (2005).
- [30] W. Bauer and G. F. Bertsch, Phys. Rev. Lett. **65**, 2213 (1990).